Meteorologische Zeitschrift, Vol. **24**, No. 3, 293–311 (published online April 4, 2015)


**Article**

# Influence of turbulence on the drop growth in warm clouds, Part II: Sensitivity studies with a spectral bin microphysics and a Lagrangian cloud model

Theres Riechelmann[1], Ulrike Wacker[2], Klaus D. Beheng[†,3], Dieter Etling[1*] and Siegfried Raasch[1]

[1]Institute of Meteorology and Climatology, Leibniz Universität Hannover, Germany
[2]Alfred Wegener Institute, Helmholtz Center for Polar and Marine Research, Bremerhaven, Germany
[3]Institute for Meteorology and Climate Research, Karlsruhe Institute of Technology, Germany

(Manuscript received April 14, 2014; in revised form November 25, 2014; accepted December 1, 2014)

**Abstract**

Raindrops in warm clouds grow faster than predicted by classical cloud models. One of the possible reasons for this discrepancy is the influence of cloud turbulence on the coagulation process. In Part I (Siewert et al., 2014) of this paper series, a turbulent collision kernel has been derived from wind tunnel experiments and direct numerical simulations (DNS). Here we use this new collision kernel to investigate the influence of turbulence on coagulation and rain formation using two models of different complexity: a one-dimensional model called RAINSHAFT (height as coordinate) with cloud microphysics treated by a spectral bin model (BIN) and a large-eddy simulation (LES) model with cloud microphysics treated by Lagrangian particles (a so called Lagrangian Cloud Model, LCM). Simulations are performed for the case of no turbulence and for two situations with moderate and with extremely strong turbulence. The idealized 0- and 1-dimensional runs show, that large drops grow faster in the case turbulence is taken into account in the cloud microphysics, as was also found by earlier investigations of other groups. For moderate turbulence intensity, the acceleration is only weak, while it is more significant for strong turbulence. From the model intercomparison it turns out, that the BIN model produced large drops much faster than the LCM, independent of turbulence intensity. The differences are larger than those due to a variation in turbulence intensities. The diverging rate of formation of large drops is due to the use of different growth models for the coagulation process, i.e. the quasi-stochastic model in the spectral BIN model and the continuous growth model in LCM. From the results of this model intercomparison it is concluded, that the coagulation process has to be improved in future versions of the LCM. The LES-LCM model was also applied to the simulation of a single 3-D cumulus cloud. It turned out, that the effect of turbulence on drop formation was even smaller as the turbulence within the cloud was weaker than prescribed in the idealized cases. In summary, the use of the new turbulent collision kernel derived in Part I does enhance rain formation under typical turbulence conditions found in natural clouds but the effect is not very striking.

**Keywords:** turbulence, spectral bin model, Lagrangian cloud model, drop collision

## 1 Introduction

The question why atmospheric raindrops grow faster in clouds than predicted by classical models has attracted attention for a long time, and turbulence effects have been suggested as a plausible mechanism (e.g., Vaillancourt and Yau, 2000). During recent years the potential acceleration of the warm-rain formation process due to turbulence effects on the coagulation growth of drops has been investigated by various authors, see the comprehensive review of Grabowski and Wang (2013). One line of research is to investigate the turbulence effects on the collision efficiency (e.g., Pinsky et al., 2001; Wang et al., 2008), the other line concentrates on the modification of the geometric collision kernel (i.e. the collection volume per time due to the differential sedimentation velocity of the drops) by turbulence induced drop clustering and superimposed motion (e.g., Ayala et al., 2008a,b; Kunnen et al., 2013). Both lines perform their calculations by theory and/or direct numerical simulations (DNS). All studies show indeed that the collision efficiency and the collision kernel increase due to turbulence effects. Numerical solutions of the kinetic collection equation for the drop size distribution (DSD) showed that, when using the new turbulent collection kernel/efficiencies (either tabulated or in parameterized form), the time to form drizzle drops is shortened compared to the turbulence-free case (Xue et al., 2008; Wang and Grabowski, 2009).

*Corresponding author: Dieter Etling, Institute of Meteorology and Climatology, Leibniz Universität Hannover, Herrenhäuser Str. 2, 30419 Hannover, Germany, e-mail: etling@muk.uni-hannover.de

†We co-authors are deeply saddened by the loss of our highly valued colleague Klaus-Dieter Beheng, who deceased on November 14, 2014.

DOI 10.1127/metz/2015/0608

Gebrüder Borntraeger Science Publishers, Stuttgart, www.borntraeger-cramer.com

Recently, the priority program METSTROEM, funded by the German Research Foundation (DFG) supported further research, that are, amongst others, (i) wind tunnel experiments to inspect the inter-particle collisions in a droplet-laden airflow of controlled turbulence intensity (Bordás et al., 2011; Bordás et al., 2012), (ii) DNS of the collision process and derivation of collision rates and kernels for various drop pairs (Kunnen et al., 2013) and (iii) large eddy simulation (LES) with a Lagrangian cloud model (LCM, Riechelmann et al., 2012). Siewert et al. (2014), henceforth called Part I, present a fit function for the turbulent enhancement of the geometric collision kernel derived from DNS. The collision rates are compared with wind tunnel measurements, where only the collisions of drops with radii larger than 7.5 µm are registered. Although the strength of turbulence varies strongly, the total collision rates match well. As a further test, the new fit function of the turbulent collision kernel has been used to simulate the evolution of the DSD numerically by solving the spectral kinetic equation (see Section 2.1) with the aim to reproduce the data as observed in the wind tunnel experiment. The initial DSD is composed predominantly of small droplets with radii less than 10 µm. Collision growth is not considered the dominant process in that size domain, hence with the turbulent kernel alone, the observed fast depletion of small drops could not be reproduced during the short observation time span of less than 1 s. This comparison suffers from the unavoidable extrapolation of the kernel data for very small droplet sizes, from the strongly different turbulence intensities in the DNS and in the wind tunnel, and from the extremely short observation time span of less than 1 s. For details see the discussion in Part I.

In the present paper (named Part II) we investigate the influence of turbulence on the coagulation growth. The effectiveness of the newly derived turbulent collision kernel function (Eqs. (4.1) to (4.6) in Part I) is now investigated for model conditions closer to situations appearing in atmospheric clouds. The differences to the indecisive similar simulations in Part I are (i) a much longer simulation time up to 2000 s and (ii) an initial drop ensemble with somewhat larger particles (droplets of average mass have a radius of 13.4 µm). Once some larger drops are formed via coagulation, the collision drop pairs have sizes comparable to those for which the kernel fit function from Part I is applicable. The sensitivity of the evolution of the DSD to the turbulence intensity will be performed with two numerical models of different complexity. They differ in geometry and in the treatment of the spatio-temporal evolution of cloud microphysical processes. These are

- the idealized RAINSHAFT model (as in Part I) with a 0-D- as well as 1-D geometry in which the spectral kinetic equation of a DSD is evaluated for many classes (bins) of drop size (therefore denoted BIN model), see Seifert and Beheng (2001); Seifert (2008), and
- the above mentioned LCM which is an LES model with a 3-D-geometry wherein the super-droplet method is applied (Riechelmann et al., 2012).

By investigating turbulence effects on the coagulation process within clouds by two different models we can also compare the performance of the newly developed Lagrangian cloud model (LCM) with respect to an established cloud physics model which solves the spectral kinetic equation for the DSD, as this has not been done before. To our surprise, the difference in the development of cloud droplets as simulated by the two models turned out much larger than the difference in simulations of the droplet development with and without turbulence effects. The reasons for this difference and possible mitigation of the problem will be given in the text.

The paper is organized as follows. In the following Section 2, the models are shortly characterized and some modifications of the LCM will be addressed. In Section 3, the sensitivity of the DSD evolution to the turbulence intensity in an idealized 0-D frame is investigated for pure coagulation, and in an idealized 1-D frame also allowing for vertical settling of drops. Finally, the sensitivity of the evolution of a shallow cumulus cloud with respect to turbulence effects is investigated with the LCM in Section 4. This is followed by the conclusions.

## 2 Methodology

In the next two subsections the two cloud microphysical modules, i.e. the spectral kinetic BIN model and the LCM model, are described.

### 2.1 The spectral bin microphysics model

A drop is characterized by its mass $x$ or equivalently by its radius $r$. The drop size number distribution DSD (or spectrum) of a drop ensemble is denoted $f_x$, where $f_x(x)dx$ is the number density of drops with masses in the interval $dx$ around $x$. In general, the DSD also depends on location $\vec{r}$ and time $t$, $f_x(x, \vec{r}, t)$, but we will skip these arguments for brevity.

In this paper, emphasis is placed on the change of the drop ensemble due to coagulation and sedimentation. Then the prognostic equation for the DSD reads (e.g., Hu and Srivastava, 1995):

$$\frac{\partial f_x(x)}{\partial t} - \frac{\partial (f_x(x) v_t(x))}{\partial z} = \frac{1}{2}\int_0^x K(x-x', x') f_x(x', t) f_x(x-x', t)\, dx' - \int_0^\infty K(x, x') f_x(x', t) f_x(x, t)\, dx' , \qquad (2.1)$$

The first term on the left hand side is the local rate of change of $f_x$, taken at constant location $\vec{r}$ and drop

mass $x$, the second gives the divergence of the sedimentation flux of $f_x$ with sedimentation velocity $v_t$. We assume that $v_t$ can be approximated by the 'terminal' velocity of a drop falling under a balance of gravity, friction and pressure forces. The right hand side stands for the source and the sink terms due to coagulation. $K(x, x')$ denotes the coagulation kernel. The droplet growth due to coagulation is treated by the quasi-stochastic growth model (see also Section 2.4), called BIN model for shortness.

The coagulation kernel carries the information on the physics of collision and coalescence of two drops. In quiescent air, the primary cause for collision is the difference in settling velocities. The gravitational coagulation kernel for drops with masses $x$ and $x'$, or likewise radii $r$ and $r'$ is given by:

$$K_{\mathrm{grav}}(r, r') = E_{\mathrm{grav}}(r, r') \underbrace{\pi (r + r')^2 \left| v_t(r) - v_t(r') \right|}_{= \Gamma_{\mathrm{grav}}(r, r')} \quad (2.2)$$

(see textbooks as e.g., Pruppacher and Klett, 1997; Rogers and Yau, 1989). $E_{\mathrm{grav}}$ is the collision efficiency for gravitational coagulation. Throughout this paper we assume – as in Part I – $E_{\mathrm{grav}} = 1$, i.e. collision of drops is followed by merging.

The evolution of the DSD according to Eq. (2.1) is numerically solved with the BIN model in the framework of a 1D-model called RAINSHAFT, used also in Part I. The terminal velocity is calculated following Beard (1976).

The vertical coordinate is discretized into equally large $\Delta z$-intervals. A simple upstream scheme is used for the sedimentation term in RAINSHAFT model.

Later, we will use the drop size distribution after a coordinate transformation, see Appendix B.

## 2.2 The Lagrangian cloud model

A Lagrangian cloud model (LCM) is a combination of a Lagrangian particle model with a large-eddy simulation (LES) model (Andrejczuk et al., 2010) or with other models providing the atmospheric flow field (velocity, temperature, pressure, specific humidity). In these models aerosols and/or drops (Lagrangian particles) are released into the flow field (e.g. simulated by LES) in order to trace their transport and evolution. Thereby the dynamics and microphysics of the cloud are directly related to the physical processes of individual drops, such as condensation, coagulation, transport and sedimentation.

The LCM used in this study was developed by Riechelmann et al. (2012) and is based on the LES model PALM (parallelized large-eddy simulation model; Raasch and Schröter, 2001) revision 1275. It was successfully applied to simulations of (precipitating) convective clouds and investigations on the influence of turbulence on raindrop growth (Riechelmann et al., 2012; Lee et al., 2014). A complete description of the LCM and the numerical methods is given in Riechelmann et al. (2012). Therefore only the basic concepts of the model and some improvements implemented in the meanwhile are described here.

In order to handle the extremely large number of aerosols and/or drops in the atmosphere computationally, an LCM simulates only a certain number $N_{\mathrm{p,total}}$ of aerosols and/or drops explicitly as Lagrangian particles. These particles are called super-droplets (Shima et al., 2009) and are indexed by an integer value, say $n$. They are treated as Lagrangian particles and move independently of the grid structure through the whole model domain. According to its size each super-droplet is interpreted as drop or, if the super-droplet radius is reduced to a size smaller than the activation radius, as wetted aerosol. Each super-droplet is assumed to represent a large number of drops of same characteristics such as size, position, and growth rate. The number of drops contributing to a super-droplet with radius $r_n$ is called weighting factor $A_n$. The weighting factor is an individual feature of each super-droplet. The initial state is defined by placing a large number of super-droplets in the model domain and by assigning each of them an initial radius $r_n$ as well as an initial weighting function $A_n$ in agreement with an initial spatial distribution of an aerosol/drop spectrum. During the simulation, $A_n$ and $r_n$ (or mass $x_n = 4/3\,\pi\rho_l r_n^3$ with liquid water bulk density $\rho_l$) of the $n$-th super-droplet change with time due to cloud microphysical processes such as coagulation.

Within the LCM, the fields of liquid water content $L(t, \vec{r})$ and of drop number concentration $N(t, \vec{r})$ can be obtained from the spatial distribution of the super-droplets at some time t. To calculate these quantities for a particular grid volume $\Delta V$ in the model domain, only those $N_p$ super-droplets are relevant which are currently in the grid box under consideration. We number them by $n = 1, \ldots, N_p$ according to their size. The number density follows as

$$N = \sum_{n=1}^{N_p} A_n / \Delta V \quad (2.3)$$

and the liquid water content as

$$L = \sum_{n=1}^{N_p} A_n x_n / \Delta V = \sum_{n=1}^{N_p} M_n / \Delta V\,, \quad (2.4)$$

where $M_n = A_n x_n$ is the total mass of the $A_n$ drops with mass $x_n$ which are represented by the $n$-th super-droplet.

The motion of each super-droplet within the turbulent flow field is calculated in the standard version directly by integrating the equation of motion for the drop. This calculation is identical to the calculations of the droplet motions in the DNS model in Part I of this paper and also includes the non-linear correction of the classical Stokes drag following Clift et al. (1978) which is especially relevant for droplet sizes $r > 30\,\mu$m. However, for comparisons with the spectral BIN model in

Section 3, the terminal velocities of the drops in the LCM are calculated following Beard (1976).

The growth due to condensation is calculated using the so-called diffusion growth rate for a drop at rest as given by Mason (1971). Since this study concentrates on the growth of cloud droplets and raindrops, solution and curvature effects on the drop's equilibrium vapor pressure are neglected. In addition to the model version described in Riechelmann et al. (2012) the so-called ventilation effect is now implemented for the evaporation of large drops ($r > 40\,\mu m$), using the ventilation coefficient $f_v$ as given by Rogers and Yau (1989):

$$f_v = 1.00 + 0.09 Re_p \quad \text{for } Re_p \leq 2.5 \text{ and} \tag{2.5}$$

$$f_v = 0.78 + 0.28 Re_p^{1/2} \quad \text{for } Re_p > 2.5\,. \tag{2.6}$$

$f_v$ is a function of the drop Reynolds number $Re_p$. The flow field information (temperature, specific humidity, velocity, etc.) necessary for the calculation of the microphysical processes are simulated by the LES and interpolated from the surrounding eight grid points to the current super-droplet position inside the grid volume. Owing to this, different super-droplets can grow differently even if they have initially the same microphysical properties.

A super-droplet that collides with smaller droplets, grows by incorporating their masses. The mass growth rate equation is given in (5.1) with the coalescence efficiency set equal to one. The growth rate of the super-droplet depends on the number of smaller drops in the respective grid box (but irrespective of their actual position), the size of the droplets and the turbulence conditions. Coagulation modifies the radius $r_n$ and the weighting factor $A_n$ of each super-droplet due to growth and depletion. Note that the drop coagulation does not lead to the creation of new super-droplets. The basic concept assumed here to model coagulation, named 'continuous model', differs from the BIN model used in the RAINSHAFT model. This is further explicated in Section 2.4.

A particular problem is the treatment of coagulation of equally sized drops. In the context of the super-droplet model, we will name the coagulation of two drops belonging both to the ensemble represented by a super-droplet as 'internal coagulation' for shortness. If the pure gravitational kernel from Eq. (2.2) is adopted, the problem does not occur, because the kernel vanishes for equally sized drops. Matters are different when the kernel accounts for turbulence effects.

In the original model described in Riechelmann et al. (2012) the chosen numerical implementation of the coagulation process revealed several shortcomings. Firstly, the prognostic cloud physical properties were the weighting factor $A_n$ as well as the radius $r_n$. The use of $r_n$ instead of the drop mass $x_n$ introduces unnecessary numerical errors. As an example, the parameter $\alpha$ introduced in that paper, becomes independent of all the weighting factors of the collected drops, if $x_n$ is used instead of $r_n$. Secondly, the integration for all super-droplets was done successively by starting with the collision of the largest super-drop $n = N_p$ with the smaller ones and consequently updating the $A_m$ ($m < n$) for each $n$ before calculating the growth of the second-largest super-drop and so on. Thirdly, internal coagulations were neglected.

These points are now modified. The prognostic variables are switched to the weighting factor $A_n$ and the mass $M_n$ of all drops belonging to the ensemble represented by the $n$-th super-droplet. Thereby mass conservation is naturally ensured. Drop mass is diagnosed from $x_n = M_n/A_n$, and hence we find the drop radius $r_n$. The previous intermediate updates of the $A_m$ are skipped. As a positive side effect, these two modifications enable a numerically more efficient integration cycle.

Furthermore, internal coagulation is now allowed. The total mass $M_n$ of all drops represented by the $n$-th super-drop remains invariant during this process, while the weighting factor $A_n$ decreases proportional to the number of collisions, that is $1/2\,A_n(A_n - 1)$. The change of $A_n$ within time interval $\Delta t$ for the grid volume $\Delta V$ follows as:

$$(\Delta A_n)_{int} = K(r_n, r_n)\frac{1}{2}A_n(A_n - 1)\frac{\Delta t}{\Delta V} \tag{2.7}$$

The full set of equations for the change of $A_n$, $M_n$ due to all coagulation processes as well as the diagnosis of $x_n$ and $r_n$ are given in the Appendix. $A_n$ decreases due to internal coagulation and collection of the drops by larger drops. $M_n$ increases due to the collection of smaller droplets and decreases due to the consumption by larger ones.

The cloud physical processes affect the fluid motion due to the release of latent heat during condensation and evaporation. These effects are computed from the size changes of the super-droplets and are included in the prognostic equations of the LES. The LES model PALM solves the non-hydrostatic incompressible Boussinesq equation, the equations for the conservation of mass, energy and moisture and a prognostic equation for the sub-grid scale turbulent kinetic energy.

## 2.3 The turbulent collision kernel

Turbulence enhances the chance that two drops collide. In part I (Siewert et al., 2014), the derivation of a coagulation kernel for turbulent conditions was described. The dissipation rate $\epsilon$ was taken as measure of the strength of turbulence. We use here the same expression for the kernel as given in Eqs. (3.3) to (3.8) in Part I:

$$\begin{aligned}\Gamma_{turb}\left(r[\mu m], r'[\mu m], \epsilon[cm^2\,s^{-3}]\right) = \\ \Gamma_{grav}(r, r')\,\eta_g(r', r - r', \epsilon) + \\ \chi(r', r - r', \epsilon)\,\Gamma_{grav}(r' + 5, r')\,\eta_g(r', 5, \epsilon)\end{aligned} \tag{2.8}$$

with $r \geq r'$ and the following parameters:

$$\begin{aligned}\eta_g(r', \alpha(r - r', \epsilon), \mu(r - r', \epsilon), \sigma(r - r', \epsilon)) = \\ 1 + \frac{\alpha}{(2\pi\sigma^2)^{0.5}}\exp\left(-\frac{(r' - \mu)^2}{2\sigma^2}\right)\end{aligned} \tag{2.9}$$

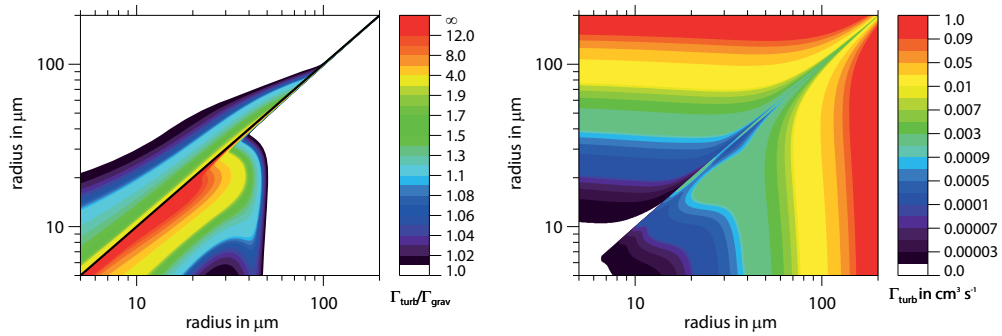


**Figure 1:** Ratio of the turbulent geometric collision kernel to the gravitational geometric collision kernel (left) and turbulent geometric collision kernel (right) for flow dissipation rates of 250 $cm^2s^{-3}$ and 50 000 $cm^2s^{-3}$ in the upper-left and lower-right part of the figure, respectively. The ratio on the diagonal in the left figure is undefined since the gravitational geometric collision kernel is zero for droplets of the same size.

$$\alpha\,(r - r', \epsilon) = 16.88 \exp(-0.184(r - r'))\epsilon^{0.2852} \quad (2.10)$$

$$\mu\,(r - r', \epsilon) = (-0.0052(r - r')^2 + 0.145(r - r') + 3.5)\,\frac{3.8\epsilon + 1915}{\epsilon + 85} \quad (2.11)$$

$$\sigma\,(r - r', \epsilon) = \frac{(r - r') + 155}{(r - r') + 25}\,\frac{\epsilon + 1300}{\epsilon + 166} \quad (2.12)$$

$$\chi\,(r', r - r', \epsilon) = \exp(-(r - r')^2)\,\frac{60r'}{r'^2 - 47.44r' + 1713}\,\frac{\epsilon}{\epsilon + 1848} \quad (2.13)$$

$r$ and $r'$ are in given in units of µm, and $\epsilon$ in $cm^2s^{-3}$. Please note that in the limiting case of turbulence-free air ($\epsilon = 0$) the turbulent kernel becomes equal to the gravitational kernel, $\Gamma_{turb}(\epsilon = 0) \equiv \Gamma_{grav}$.

The analytic function for the turbulent collision kernel was derived for dissipation rates up to $\epsilon = 250\,cm^2s^{-3}$. These dissipation rates match well those observed in real cumulus clouds. In situ observations by Siebert et al. (2006) and Katzwinkel et al. (accepted) have found average values of about $\epsilon = 100\,cm^2s^{-3}$ but with a large variation within single clouds in the range $\epsilon = 10$–$1000\,cm^2s^{-3}$. A typical value for cloud free areas outside clouds is about $\epsilon = 1\,cm^2s^{-3}$. In the following we present also simulations with a much higher dissipation rate of $\epsilon = 50\,000\,cm^2s^{-3}$ which is not realistic for turbulence in cumulus clouds. This dissipation rate is taken in order to investigate the effect of turbulence on the coagulation process for an extreme case. The value 50 000 has been chosen because this was a typical dissipation rate in the wind tunnel experiments described in Part I (Siewert et al., 2014). It should be noticed, however, that the application of the analytic function for the turbulent collision kernel as given by equations (2.8–2.13) to such extreme dissipation rates is merely by extrapolation.

In Fig. 1 the ratio $\Gamma_{turb}/\Gamma_{grav}$ and $\Gamma_{turb}$ are plotted as function of the radii of the colliding drops. Thereby the upper left parts of the figures are calculated for a flow dissipation rate of $\epsilon = 250\,cm^2s^{-3}$ and the lower right parts of the figures for $\epsilon = 50\,000\,cm^2s^{-3}$, respectively.

The ratio $\Gamma_{turb}/\Gamma_{grav}$ in Fig. 1(a) presents the enhancement of the gravitational kernel due to turbulence effects. The ratio is undefined along the diagonal since $\Gamma_{grav}$ is zero for drops of the same size, see Eq. (2.2). The figure shows, that noteworthy enhancements due to turbulence only occur for drops with $r < 100$ µm since the motion of larger drops is dominated by the gravitational settling. In general, the enhancement factor decreases with increasing drop size and with decreasing turbulence intensity. An exception is for larger drops (here for $r > 40$ µm) where the enhancement is stronger in case of the lower dissipation rate. A similar behavior was also observed for the kernel from Ayala and Wang in Wang and Grabowski (2009) and is due to stronger clustering of those particles.

The turbulent collision kernels in Fig. 1(b) vary over several orders of magnitude for both selected values of $\epsilon$. The kernel is dominated by the contribution of the gravitational kernel for large drops, that is $\Gamma_{turb}/\Gamma_{grav} \to 1$ (as $\Gamma_{turb}$ includes $\Gamma_{grav}$, see equations (2.8ff)).

## 2.4 Differences in the concepts for the coagulation model

Beside the fact, that the models RAINSHAFT/BIN and LES/LCM differ in their objectives, i.e. 1-dimensional idealized model for cloud microphysics versus 3-dimensional model for convective clouds with full dynamics, they also differ in the concept of treating pure coagulation. In LCM, the superdroplets (index $n$), each of which

represents many ($A_n$) drops of mass $x_n$, grow all at exactly the same rate given in Eq.(5.1). We refer to this concept as the continuous model following Gillespie (1975).

In RAINSHAFT with the BIN model, only a fraction of drops from a certain mass interval around mass $x$ collect smaller droplets of mass $x'$, while others collect droplets of different mass or perhaps none at all; thereby the drops grow at different growth rates. This concept is called the quasi-stochastic model by Gillespie (1975). He used 'quasi' to straighten the lack of any probabilistic element. Gillespie shows that the quasi-stochastic model leads to a faster evolution of the drop size spectrum such that larger drops are formed earlier than in the continuous model. There is always an at least small fraction of drops from the mass interval around $x$ which grow much faster the other drops from this interval. Thus some much larger drops are formed, and their presence will again speed up the formation of even larger drops.

When comparing results from the LCM and the BIN model, one should hence expect that larger drops develop faster in the latter model. Indeed, this is clearly seen in the results presented in Section 3. It is already mentioned here that the differences in drop spectrum development between both models are larger than the differences between the model runs with and without turbulence effects. This relatively large impact has not been foreseen by the authors when starting their study, as no comparison between their LCM and a more classical cloud physics model has been performed before. Hence this study revealed a shortcoming of the present treatment of coagulation growth in the LCM.

In order to mitigate this shortcoming, it will be necessary to modify or exchange the continuous growth model. One way is to modify the continuous model by adding a new super-droplet characteristic which includes a variance information for the droplet size. This variance could be calculated by introducing a Gaussian noise after the new super-droplet size is calculated. Using this method should improve the formation of larger drops at relatively low numerical cost. Another possibility is to exchange the continuous model by enabling the generation of new super-droplets during the coagulation process, similar to the method used by Andrejczuk et al. (2010). In order to keep the total number of super-droplets and thus the numerical cost at a manageable level, super-droplets with similar size and locations have to be merged. The implementation and test of those methods is currently under investigation for the LCM presented here.

# 3 Case studies for idealized configurations

## 3.1 Setups

**(a) Case 1: Coagulation**

This case is intended to analyze the influence of the turbulent geometric collision kernel given in Eqs. (2.7) to (2.12) and presented in Part I on the evolution of the drop spectrum due to coagulation alone. This is achieved by neglecting all other processes like advection, sedimentation and droplet growth due to condensation etc. in the model. We choose the three turbulence conditions as in Part I: turbulent dissipation rate of $\epsilon = 0$, i.e. the pure gravitational kernel, $\epsilon = 250\,\mathrm{cm^2 s^{-3}}$ and $\epsilon = 50\,000\,\mathrm{cm^2 s^{-3}}$ as discussed in Subsection 2.3. The initial DSD is given by a gamma distribution

$$f_r(r, t = 0) = B\, r^{\nu-1} \exp(-\lambda r) \tag{3.1}$$

with $\nu = 16$, as shown in Fig. 2. The liquid water content is set to $L_0 = 10^{-6}\,\mathrm{g\,cm^{-3}}$ and the droplet number concentration is $N_0 = 100\,\mathrm{cm^{-3}}$, thus the radius of a drop with initial mean mass $\overline{x}_0 = L_0/N_0$ is $\overline{r}_0 = (3\overline{x}_0/4\pi\rho_l)^{1/3} = 13.4\,\mu\mathrm{m}$ with bulk density of liquid water $\rho_l = 1\,\mathrm{g\,cm^{-3}}$. The minimum radius in both models is set as $r_{\min} = 1\,\mu\mathrm{m}$. The high $\nu$-value is chosen to start with a narrow initial spectrum, such that the increase of the collision kernel due to turbulence effects, which is strongest for droplets of similar sizes (Fig. 2), should have a large impact.

The simulation time is 2000 s with a time step of 1 s for the two microphysical models. In the BIN model, the radius coordinate $r$ is logarithmically discretized into 160 bins of equal $\Delta \ln r$-intervals. Since the LCM is a three-dimensional model, the evolution of $f_r$ inside a single grid volume ($\Delta x = \Delta y = \Delta z = 50\,\mathrm{m}$) is analyzed. In this grid volume the initial drop ensemble is represented by a total of 1000 super-droplets, in such a way the radius coordinate $r$ is also discretized into 1000 bins of equal $\Delta \ln r$-intervals, and each bin is represented by one super-droplet. This large number of super-droplets is chosen to reduce statistical fluctuations in the large drop range for the comparison with the results of the spectral bin model. The spatial distribution of the super-droplets does not matter in this case since advection is neglected.

**(b) Case 2: Coagulation and sedimentation**

In this second case study we analyze the influence of the turbulent collision kernel on the drop growth due to coagulation while the droplets are allowed to settle in the field of gravity. We use the two microphysical models presented in Sections 2.1 (BIN in 1-D RAINSHAFT) and 2.2 (LCM in 3D LES).

The setup is one-dimensional with the vertical coordinate $z$, in which a box-shaped cloud is initialized between 2000 m and 4000 m. The cloud is characterized by the same initial drop spectrum and the simulations are performed for the same three turbulent dissipation rates as in the first case. The vertical grid spacing is 50 m for both models geometries. To represent the one-dimensional setup in the three-dimensional LCM one vertical column (50 m × 50 m × 4000 m) is taken as model domain. The simulation time is 4000 s with a time step of 1 s. Different to the previous case, the initial droplet spectrum is represented in the LCM by 2000

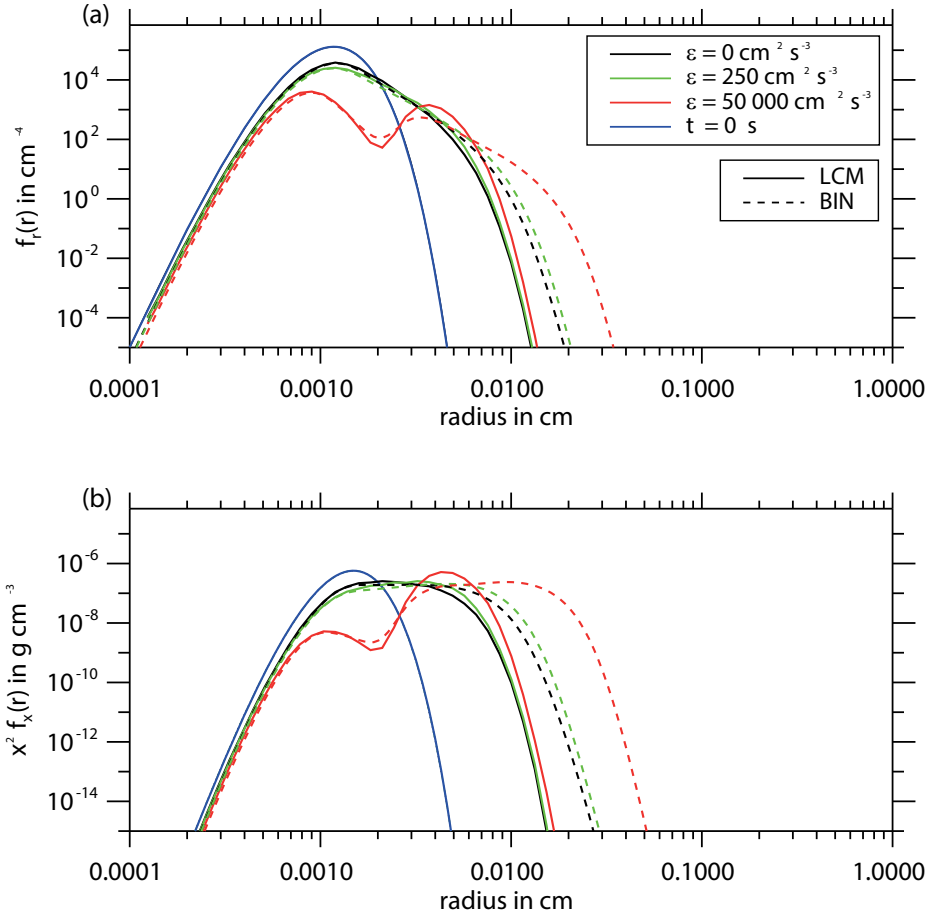


**Figure 2:** Number (a) and mass (b) density distributions after $t = 500$ s of the spectral BIN model (dashed) and the LCM (solid) for the three turbulent conditions $\epsilon = 0$ (black), $\epsilon = 250\,\mathrm{cm^2 s^{-3}}$ (green) and $\epsilon = 50\,000\,\mathrm{cm^2 s^{-3}}$ (red) for case 1 (coagulation). The blue lines represent the initial distributions.

super-droplets per grid volume, which are released with a horizontal distance of 25 m and a vertical distance of 0.1 m. The arrangement of the super-droplets into four vertical colomns within a grid box is due to computational reasons. By using a small vertical distance a continuous vertical distribution of the super-droplets is achieved. We used a larger number of super-droplets per grid volume in this case to reduce sampling issues which arise when only a small number of super-droplets are distributed over a large domain.

## 3.2 Results case 1: Coagulation

The evolution of the drop spectrum after $t = 500$ s, $t = 1000$ s and $t = 2000$ s for the three turbulent conditions and both models (BIN and LCM) is shown in Figs. 2 and 3. The upper panels show the distribution of the number concentration per radius interval $f_\mathrm{r}$, the lower panels show the distribution of the mass density function per logarithmic mass interval, as defined in Appendix B, both plotted as function of the drop radius $r$. In all cases one recognizes that coagulation produces larger drops at the expense of the smaller ones, and the number of drops is strongly reduced.

First we compare the results from the two models for the case of turbulence free conditions. The corresponding black solid and dashed lines differ in a systematic way, showing that the BIN model leads to a faster formation of large drops than the LCM. This is due to the quasi-stochastic growth model, used in BIN, and the continuous growth model, used in LCM, as already indicated in Subsection 2.4. The difference between the two models is independent of the turbulence strength.

We now turn to the influence of the turbulence on coagulation. Both models show, that the drops grow faster with increasing $\epsilon$. For the extreme case of $\epsilon = 50\,000\,\mathrm{cm^2 s^{-3}}$ the depletion of drops of radii between 10 and 20 µm is so fast, that for both distribution functions $f_\mathrm{r}$ and $x^2 f_\mathrm{x}$ a relative minimum develops near $r = 20$ µm already after 500 s, and strengthens later on. Turbulence primarily increases the collision kernel for small drop sizes, see Fig. 1. With larger dissipation rates $\epsilon$, the coagulation process of particularly small drops is accelerated. The earlier occurrence of the resulting larger drops enhances further growth by depletion of the smaller ones in this unstable colloid system.

Though we find an overall speed up of the formation of large drops for $\epsilon = 250\,\mathrm{cm^2 s^{-3}}$, a dissipation rate typical in clouds, the impact is only moderate. A comparison with the sensitivity found by e.g., Xue et al. (2008) is impeded due to different model assumptions.

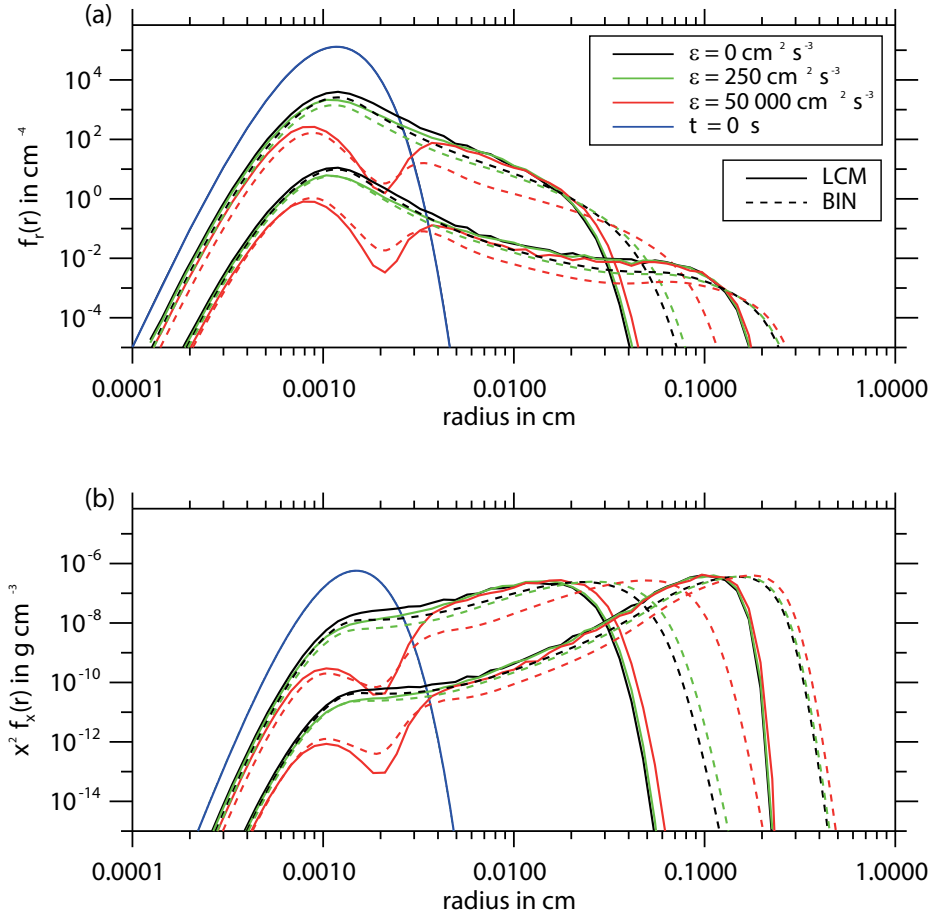


**Figure 3:** Same as Fig. 2, but for $t = 1000$ s and $t = 2000$ s. Results for the different times are distinguished as the spectrum contains many more small droplets and less large drops at $t = 1000$ s than at $t = 2000$ s.

Amongst are the differing initial spectra and the assumption of a collision efficiency of $E_{\text{coll}}$=1 in the present paper; the latter is motivated by the fact, that no efficiency had been derived in Part I. In a comparative study using the same initial conditions and collision efficiency according to (Hall, 1980), we find a similar evolution under the turbulence-free conditions; differences are due to different numerical implementation of the nonlinear prognostic equation (2.1). In the turbulent case, Xue et al. (2008) find a faster formation of large drops than in the turbulent-free case. We estimate that the differences shown in Figs. 10 and 11 in Xue et al. (2008) are somewhat larger than seen in the present Figs. 2 and 3 for $\epsilon = 250\,\text{cm}^2\text{s}^{-3}$ and level out if selecting their $\epsilon = 300\,\text{cm}^2\text{s}^{-3}$. But it turns out, too, that the selection of the collision efficiency has a great impact.

Since the collision kernel ist most strongly affected for small droplets (Fig. 2), it is expected that the sensitivity to turbulence intensity is stronger for larger contribution of small droplets in the initial drop ensemble, and vice versa. Increasing the initial number of drops by, e.g., a factor of 10 compared to the case discussed above, thus assuming a continental situation with smaller average drop mass, indeed results in a stronger influence of turbulence intensity. Some of the differences in sensitivity in comparison with Xue et al. (2008) stems probably from the somewhat smaller initial average drop mass compared to the case presented here.

**Table 1:** Time after which in case 1 50 % of the cloud water content $L_{\text{cloud}}$ is converted to rain water content $L_{\text{rain}}$ for the three turbulent conditions and both models.

| | $\epsilon = 0$ | $\epsilon = 250\,\text{cm}^2\text{s}^{-3}$ | $\epsilon = 50\,000\,\text{cm}^2\text{s}^{-3}$ |
|---|---|---|---|
| BIN | 613 s | 537 s | 258 s |
| LCM | 724 s | 646 s | 390 s |

To get a more general overview of the influence of the turbulent geometric collision kernel and the differences between the models over the course of time, Fig. 4 shows the time series of the total $N_{\text{tot}}$, cloud $N_{\text{cloud}}$ and rain $N_{\text{rain}}$ droplet number density and of the total liquid $L_{\text{tot}}$, cloud $L_{\text{cloud}}$ and rain $L_{\text{rain}}$ water content. Here drops with $r \geq 40\,\mu$m are interpreted as raindrops and smaller ones as cloud droplets. Since drop advection and sedimentation are neglected in this case, $L_{\text{tot}}$ is constant and $N_{\text{tot}}$ decreases with time.

Again, both models show that the generation and growth of raindrops is faster and that the maximum number of raindrops during the simulation is larger when using the turbulent geometric collision kernel. The largest effect is seen for the extreme case of $\epsilon = 50\,000\,\text{cm}^2\text{s}^{-3}$.

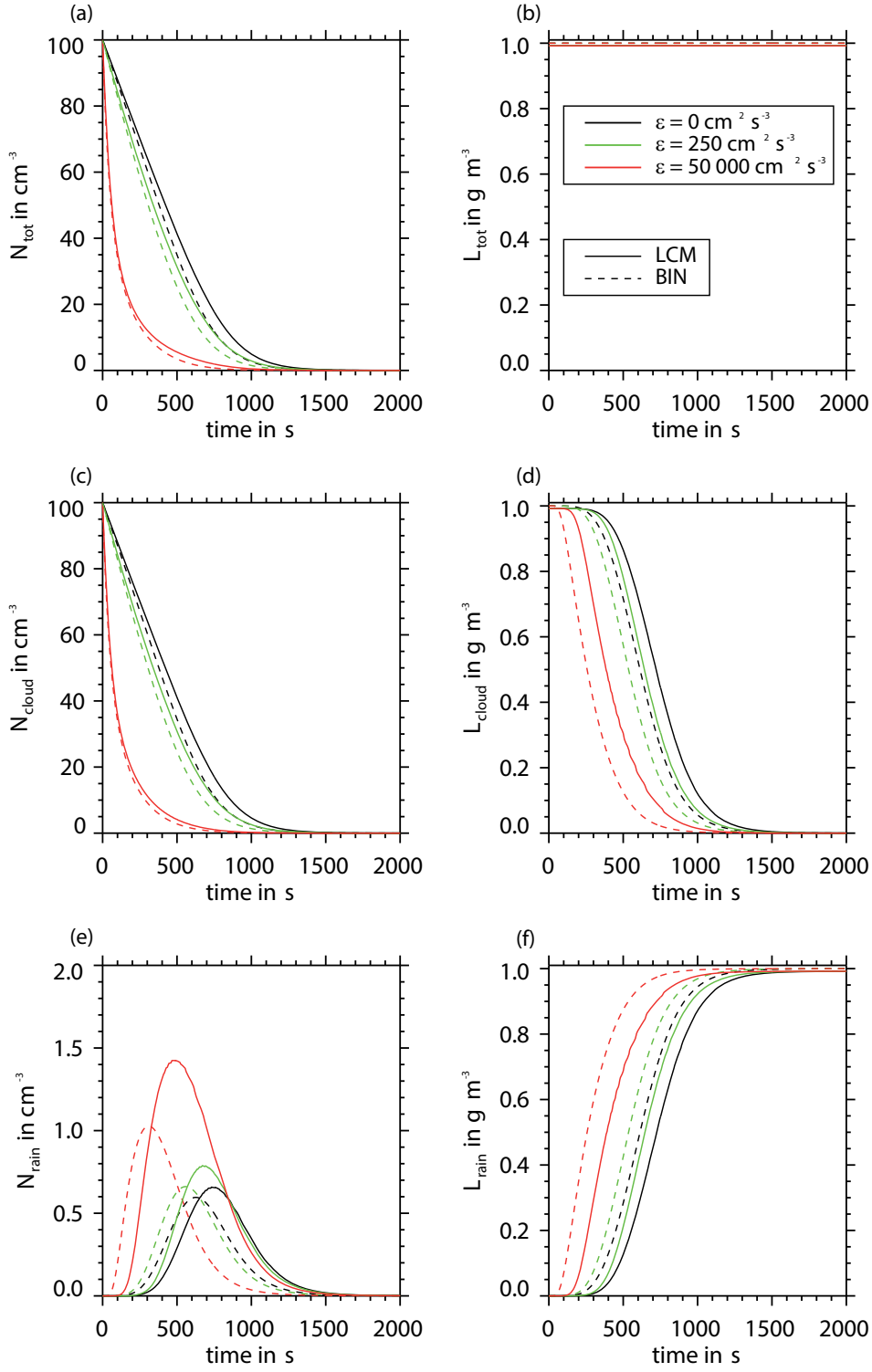


**Figure 4:** Time series of the total (a), cloud (c) and rain (e) droplet number density and of the total liquid (b), cloud (d) and rain (f) water content of the spectral BIN model (dashed) and the LCM (solid) for three turbulent conditions $\epsilon$ for case 1 (coagulation).

To quantify the enhancement, Table 1 shows the simulation time at which 50 % of the cloud water content $L_{\text{cloud}}$ is converted to rain water content $L_{\text{rain}}$ for the three turbulence conditions and both models. For $\epsilon = 50\,000\,\text{cm}^2\text{s}^{-3}$ the time needed for the conversion is 58 % shorter for the BIN and 47 % shorter for the LCM model compared to the respective simulation with gravitatonal kernel. For $\epsilon = 250\,\text{cm}^2\text{s}^{-3}$ the conversion time is reduced by 13 % (BIN) and 11 % (LCM) respectively. The growth of the raindrops is slower in the LCM due to the use of the continuous growth model for coagulation as already discussed (see also Section 2.4). Table 1 shows, that for the simulations with gravitational kernel and moderate turbulence this effect ex-

tends the conversion times of the LCM by almost 20 %. For $\epsilon = 50\,000\,\mathrm{cm^2 s^{-3}}$ this effect is even larger due to the nonlinearity of the coagulation growth and the time needed for the conversion is 50 % larger for the LCM as compared to the BIN model.

### 3.3 Results case 2: Coagulation and sedimentation

In Figs. 5 to 7 vertical profiles of the number densities and liquid water contents are presented. As in Section 3.2 we split these integral properties into the contributions from the cloud droplets and from the raindrops. The profiles are depicted for three different simulation times: 500 s, 1000 s and 2000 s, respectively. As in Section 3.2, three different collision kernels are considered depending on the turbulent dissipation rate $\epsilon$. The vertical range of the initial cloud is marked by a bold solid black line in each figure.

Firstly, we discuss the general appearance of the results as function of simulation time without distinguishing between BIN and LCM and different $\epsilon$.

After 500 s (Fig. 5) the cloud number density $N_{\mathrm{cloud}}$ and liquid water content $L_{\mathrm{cloud}}$ are still concentrated in the cloud's body accompanied by a more or less strong decrease of the number densities of cloud droplets and a negligible change of the initial cloud profile (first row). Only few raindrops have formed and are located at the cloud's edge. Their liquid water contents $L_{\mathrm{rain}}$ follow in shape the number densities (second row). Sedimentation has not yet been working efficiently till that time.

This picture has changed after 1000 s simulation time (Fig. 7). The number densities of cloud droplets have diminished dramatically and the correponding liquid water contents have decreased from initially $1\,\mathrm{g\,m^{-3}}$ to about less than $0.1\,\mathrm{g\,m^{-3}}$. The number densities of raindrops are equally reduced but with an appreciable number below the initial cloud base at 2000 m. The liquid water contents have strongly changed as the drops have moved downwards (also below the initial cloud base). At that instant sedimentation starts working efficiently.

After 2000 s (Fig. 7) there is nearly no similarity to the previous figures. Cloud droplets nearly disappeared completely except in the cloud top region. Raindrops are very scarce in number throughout the vertical cloud column, and once again near cloud top some raindrops remain. The raindrop liquid water contents show a nearly linear increase from a region near cloud top to the surface with the largest values not exceeding $0.4\,\mathrm{g\,m^{-3}}$. In Fig. 8, the time series of the accumulated rain amount at the surface exhibits, that after 2000 s nearly 50 % of the maximum rain amount (2 mm) has reached the ground through sedimentation. The irregularities seen in Fig. 7 for the LCM runs will be discussed later on.

Secondly, we analyze and discuss the influence of turbulence/no-turbulence together with the results for the two applied models BIN (dashed lines) and LCM (solid lines).

The impact of turbulence is already seen after a simulation time of $t = 500\,\mathrm{s}$ in Fig. 5. The slowest decrease in number densities and liquid water contents of cloud droplets occurs for the no-turbulence case (black lines). For the moderate $\epsilon = 250\,\mathrm{cm^2 s^{-3}}$ (green lines) the loss of cloud particles is stronger relative to the no-turbulence case for number density and for cloud liquid water content. For the extreme case $\epsilon = 50\,000\,\mathrm{cm^2 s^{-3}}$ (red lines) the reduction of number density and cloud liquid water content is stronger than expected.

One also recognizes that in simulations with the BIN model the temporal change is considerably faster than with the LCM model for all cases. This effect is due to the different growth models used in BIN and LCM as already pointed out.

This behavior, exemplarily just described for the results at $t = 500\,\mathrm{s}$, is more or less the same for the times $t = 1000\,\mathrm{s}$ (Fig. 6) and 2000 s (Fig. 7) as described in the general appearance note above, but the differences for the cloud variables - considering all parameters discussed so far – are nearly beyond the resolution of the graphics in Figs. 6 and 7. As an important result of this analysis we note that the strongest effects come from the highest dissipation rate and the weakest for the no-turbulence case, and that for both models.

All what has been said for the cloud variables can also be seen – in a reverse manner – for the rain variables. The strongest increase in raindrop number density and rain liquid water content occur for the largest dissipation rate followed by a moderate increase for the $\epsilon = 250\,\mathrm{cm^2 s^{-3}}$-case and the weakest effect for the no-turbulence case.

For $t = 1000\,\mathrm{s}$ the profiles of raindrop number densities and rain water content are qualitatively equivalent to that described in the general appearance note made above. For the rain liquid water contents the turbulence influence is again strongest for the highest dissipation rate where the corresponding maximum liquid water contents differ locally by about $0.5\,\mathrm{g\,m^{-3}}$ among the two models with $0.95\,\mathrm{g\,m^{-3}}$ the largest value. Here we find the most eminent difference between the BIN and the LCM model. Generally the maximum values obtained by the BIN model are in lower levels than those obtained by the LCM model. Again the largest difference turns out to be for the highest dissipation rate (red dashed line). This contrast between the BIN and LCM results is caused by the fact that the BIN model is simulating an earlier formation of large drops than the LCM, as we have already seen for the pure coagulation case in Section 3.1. Bigger drops settle faster and hence the signal in $L_{\mathrm{rain}}$ is shifted downwards more rapidly. This effect may be superimposed by a numerical effect namely the diffusivity of the applied upstream scheme for the numerical solution of the sedimentation equation in the BIN model.

Finally we turn to the results after $t = 2000\,\mathrm{s}$. For the BIN model the lowest values of rain liquid water content

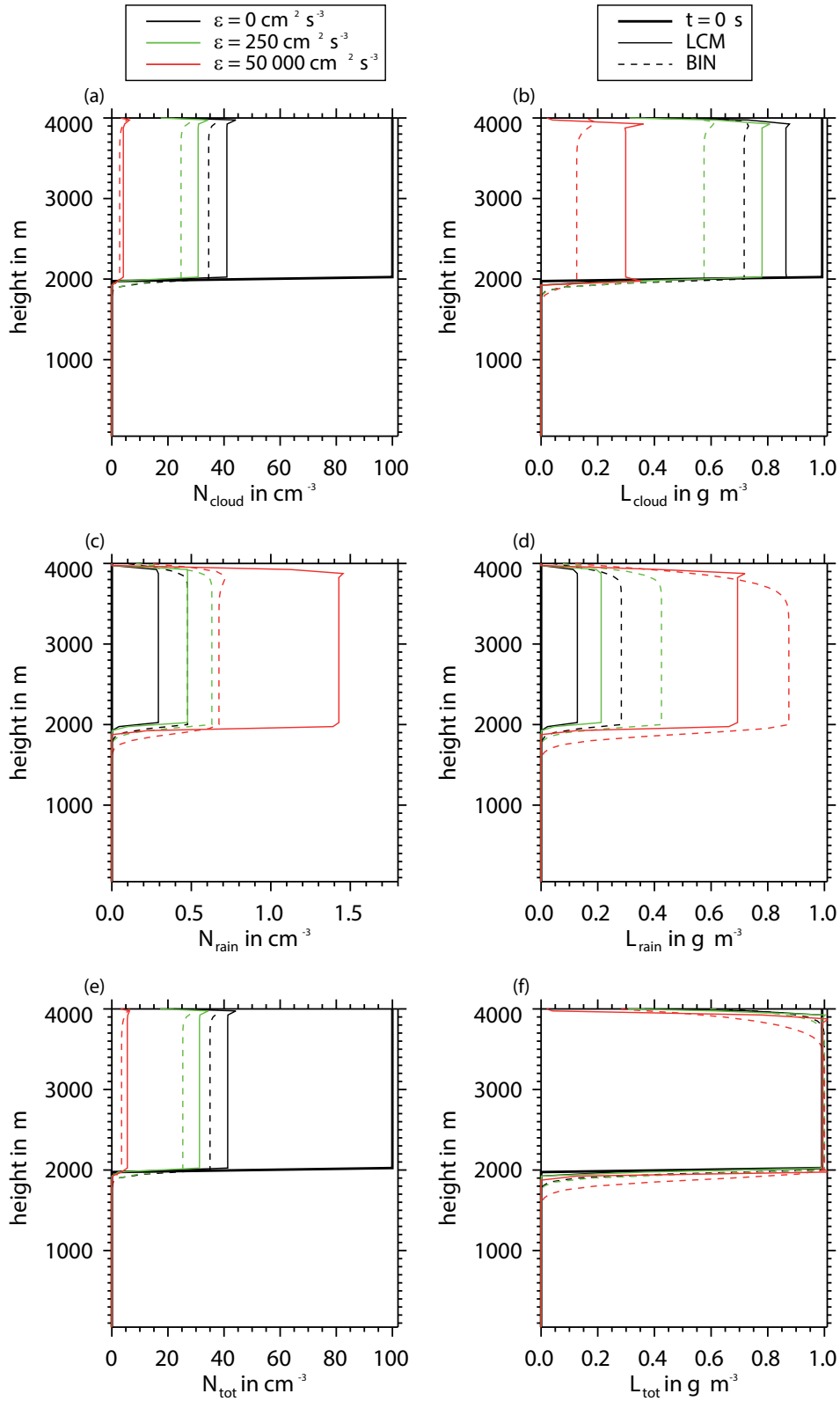


**Figure 5:** Vertical profile of the cloud (a), rain (c) and total (e) drop number density and of the cloud liquid (b), rain (d) and total (f) water content after $t$ = 500 s of the spectral BIN model (dashed) and the LCM (solid) for three turbulent conditions $\epsilon$ for case 2 (coagulation and sedimentation). The bold black lines indicate the initial distribution.

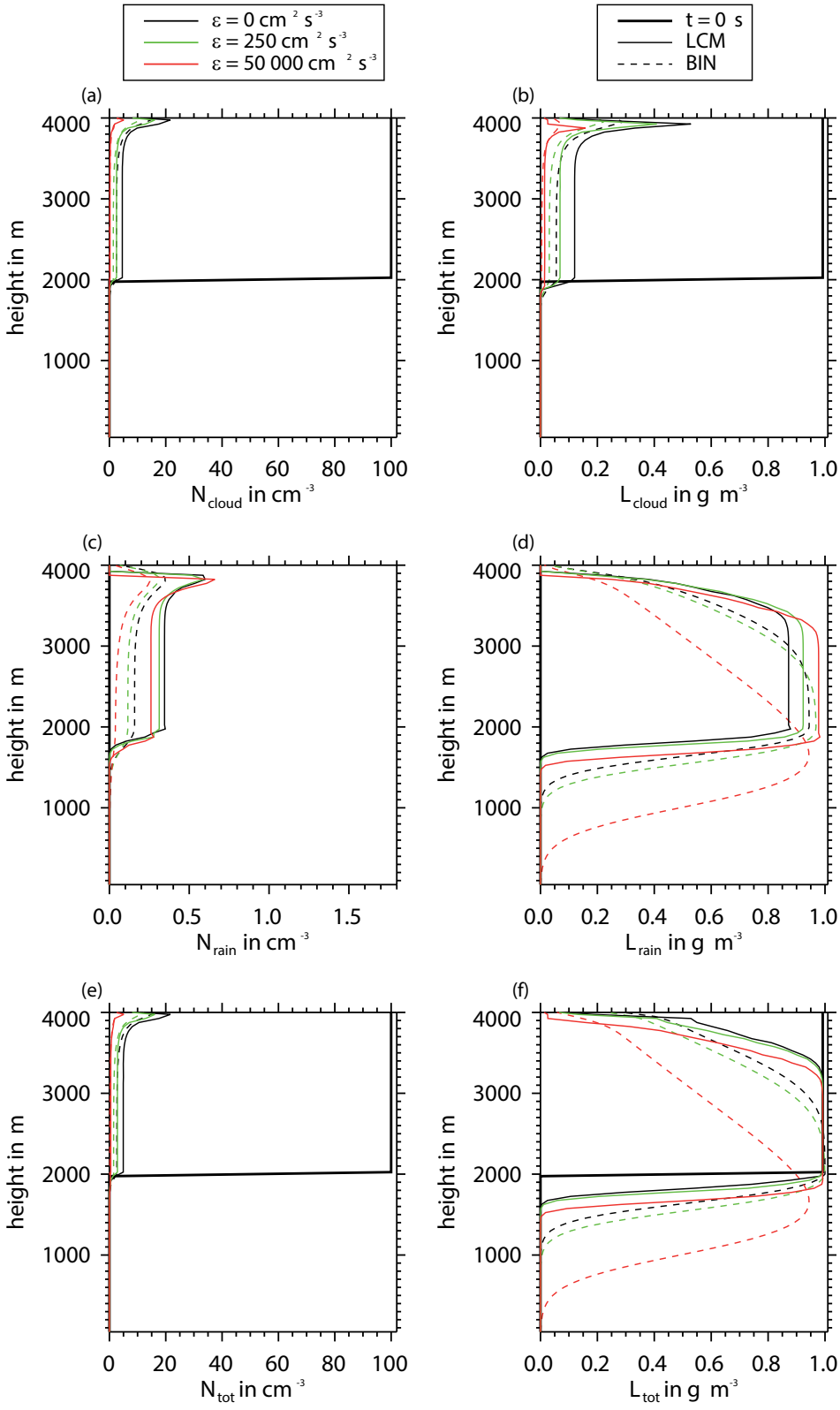


**Figure 6:** Same as Fig. 5, but for $t = 1000$ s.

correspond to the highest dissipation rate and the largest values to the no-turbulence case.

The results from the LCM model show a similar behavior, but the lines now show statistical fluctuations. The reason for these fluctuations is the small number of remaining super-droplets in the raindrop range. The profiles are calculated using the masses, weighting factors and positions of the individually advected Lagrangian super-droplets. This can lead to fluctuations if the number of corresponding super-droplets is small.

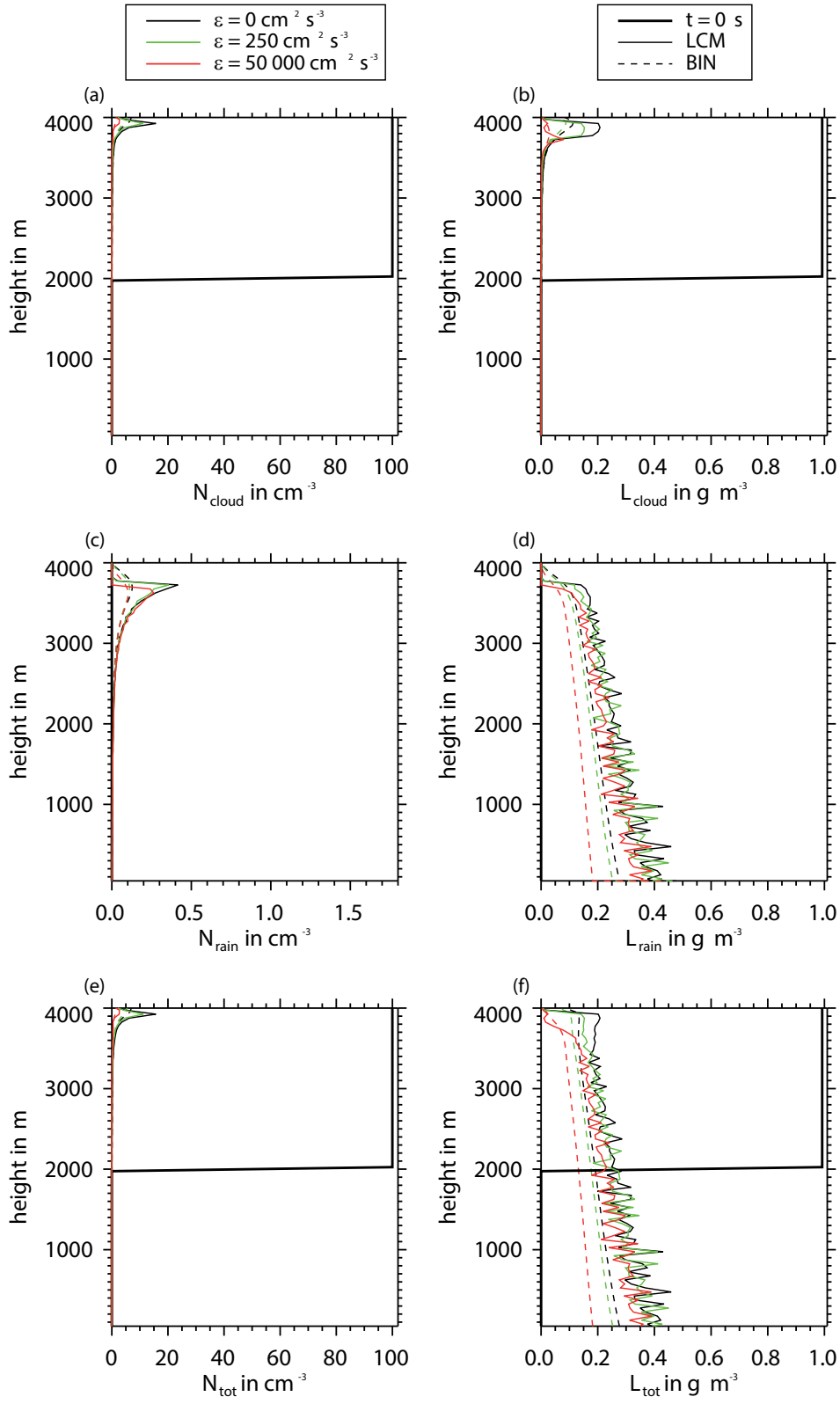


**Figure 7:** Same as Fig. 5, but for $t$ = 2000 s.

After 2000 s the number of super-droplets in the raindrop range is small because most of the rain amount has already reached the surface. The range of the fluctuations increases with decreasing height since the droplet masses increase during their sedimentation. These fluctuations can be reduced by using a higher number of initial super-droplets or by using a method proposed by Unterstrasser and Sölch (2013) in which the rare large super-droplets are divided into multiple super-droplets with reduced corresponding weighting factors.

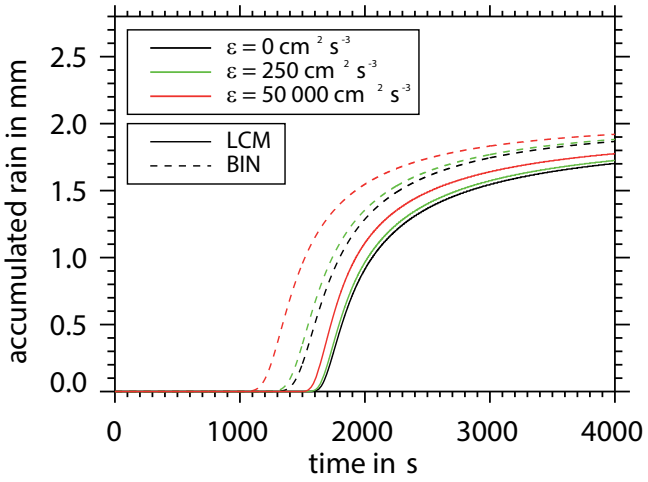


**Figure 8:** Time series of the accumulated rain amount at the surface of the spectral BIN model (dashed) and the LCM (solid) for the three dissipation rates for case 2 (coagulation and sedimentation).

This method is currently beeing implemented in the LCM used in this study.

Concerning the influence of the turbulence on the evolution of the cloud, both models show, that the drops grow faster with increasing $\epsilon$. Consequently the gravitational settling of the drops is accelerated and the cloud dissolves faster. These effects can also be seen in Fig. 8 in the time series of the accumulated rain amount at the surface for the three turbulence conditions and the two models. Again, both models show that the onset of rain starts earlier when using the turbulent geometric collision kernel, which is due to the accelerated growth of the raindrops by coagulation. As expected, the largest effect is seen for the BIN model and the extreme dissipation rate $\epsilon = 50\,000\,\mathrm{cm^2 s^{-3}}$. The later onset and the reduced amount of the accumulated rain in the LCM is a result of the slower drop growth due to the continuous growth model used for the drop coagulation, as discussed in Section 2.4.

# 4 Case 3: Idealized three-dimensional cloud

## 4.1 Setup

In this case, the influence of the turbulent collision kernel on the formation of rain drops in a developing idealized single cumulus cloud is analyzed. This simulation can only be performed with the three-dimensional LCM, where the turbulent flow field of the cloud is simulated by a LES model. The microphysical processes including the three-dimensional transport, the droplet growth due to condensation/evaporation and the droplet growth due to coagulation are treated by Lagrangian particles as described in Section 2.2. Details of the LES model are given in Riechelmann et al. (2012) and will not be repeated here.

The model domain is 1,6 km × 3,84 km × 3,84 km along the $x$, $y$ and $z$ directions with a grid spacing of 20 m. Here the grid spacing is much smaller than for the idealized cases discussed in Section 3 in since it is known that some quantities of cumulus clouds are sensitive to the grid resolution (Matheou et al., 2011).

The initial profiles of the potential temperature and the specific humidity are based on the BOMEX (Barbados Oceanographic and Meteorological Experiment; Holland and Rasmusson, 1973) shallow cumulus case and are taken from Siebesma et al. (2003). However, in contrast to Siebesma et al. (2003) no background wind, large-scale forcings or surface fluxes are used for this case. The simulation time is 1800 s and the time step is 0.1 s. The smaller time step is required in this case for the accurate calculation of droplet growth due to condensation/evaporation.

Analogue to previous simulations (Riechelmann et al., 2012; Lee et al., 2014) the idealized single cloud is initialized using a two-dimensional rising warm air bubble which is triggered by an initial potential temperature difference $\theta^*$ of Gaussian shape

$$\theta^*(y,z) = \theta_0 \cdot \exp\left[-0{,}5 \cdot \left(\left(\frac{y-y_c}{a_y}\right)^2 + \left(\frac{z-z_c}{a_z}\right)^2\right)\right]. \quad (4.1)$$

Here $y_c = 1920\,\mathrm{m}$ and $z_c = 190\,\mathrm{m}$ mark the initial center of the bubble. The temperature difference $\theta^*$ is maximum at the centre, $\theta^*(y_c, z_c) = \theta_0 = 0.2\,K$ and decreases exponentially with a standard deviation of $a_y = a_z = 150\,\mathrm{m}$. The initial warm air bubble is homogeneous in the $x$-direction.

The super-droplets are released at the beginning of the simulation and are uniformly distributed all over the model domain, up to a height of 2800 m. The average distance of the super-droplets is initially 4 m, yielding a total number of roughly $3.2 \times 10^8$ and about 125 super-droplets per grid box. Using a weighting factor of $8 \times 10^9$ for each super-droplet, an initial CCN concentration of approximately $100\,\mathrm{cm^{-3}}$ is represented, resembling a pristine maritime environment. All initial droplets have the same radius $r = 0.1\,\mu\mathrm{m}$.

The simulation is performed twice, once with the gravitational and once with the turbulent coagulation kernel presented in Section 2.3. The collision efficiency $E_{\mathrm{coll}}$ is accounted for in both cases, that is $\Gamma_{\mathrm{grav}}(r, r')$ in the turbulence-free case and $\Gamma_{\mathrm{turb}}(r, r')$ in the turbulent case are each multiplied by the same $E_{\mathrm{coll}}(r, r')$ as given in Hall (1980).

## 4.2 Results

The general evolution of an idealized single cloud simulated with our LCM was already discussed in detail in Riechelmann et al. (2012) and Lee et al. (2014) for nearly identical setups. Therefore we will give only a brief overview over the general cloud evolution and concentrate on the differences generated by the different

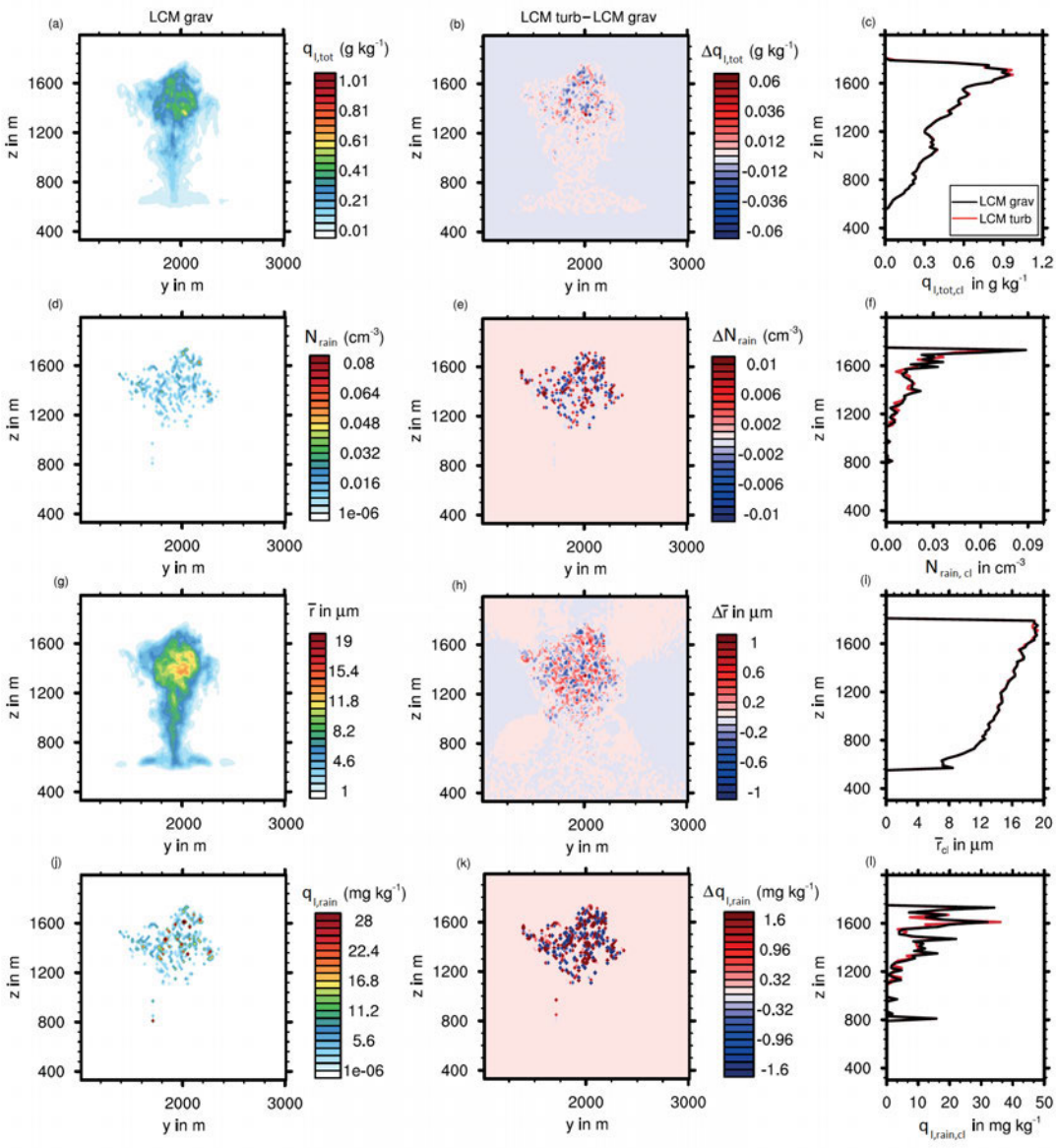


**Figure 9:** Vertical (*y*-*z*-)cross sections and profiles of the total liquid water mixing rato $q_{l,tot}$ (a-c), the average drop radius $\overline{r}$, the raindrop number density $N_{rain}$ (g–i) and the rain water mixing ratio $q_{l,rain}$ (j–l) at $t = 1600$ s. The left column shows vertical cross sections of the simulation with gravitational kernel (indicated by LCM grav), the middle column shows cross sections of the differences between the simulations with turbulent and gravitational kernel (LCM turb – LCM grav) and the right column shows vertical profiles of both simulations. The cross sections are averaged along the *x*-direction, the profiles show the horizontal average over all cloudy grid volumes, i.e. grid volumes with $q_{l,tot} > 10^{-2}$ g kg$^{-1}$), indicated by index 'cl'.

coagulation kernels. The results are presented in Fig. 9 which shows the total liquid water mixing ratio $q_{l,tot}$, the average drop radius $\overline{r}$, the raindrop number density $N_{rain}$ and the rain water mixing ratio $q_{l,rain}$ after $t = 1600$ s. The values shown in the y-z cross sections have been obtained by averaging along the *x*-direction. The vertical profiles show the horizontal average of all grid volumes classified as cloud (i.e. with $q_{l,tot} > 10^{-2}$ g kg$^{-1}$). As in the previous sections, raindrops are defined as drops with $r > 40$ µm. In this case, the dissipation rate $\epsilon$ needed for the calculation of the turbulent collision kernel (see Section 2.3) is not fixed, but calculated locally from the parameterization of the subgrid-scale turbulence in the LES model instead (see Riechelmann et al., 2012).

During the simulation, the rising warm air bubble generates an idealized single cloud with a life span of about 2100 s, of which the first 1800 s are discussed here. The cloud starts to form after approximately 550 s due to the initial updraft of the warm air bubble with vertical velocities of approximately 2 ms$^{-1}$. Raindrops are initiated after about 1000 s when the convective cloud is fully developed. The mean value of the dissipation rate $\epsilon$ in the cloud at this stage is about 40 cm$^2$s$^{-3}$ with maximum values of 80 cm$^2$s$^{-3}$. This is within the range observed for small cumulus clouds (e.g., Siebert et al.,

2006; Katzwinkel et al., accepted), but much smaller than the values used in the idealized simulations presented in Section 3.

In the further course of the simulation the cloud reaches the inversion layer, spreads horizontally and is increasingly influenced by entrainment and mixing of surrounding dry air. These effects can be seen in Fig. 9, especially close to the cloud edges. During that stage, the cloud has reached its maximum size and contains the maximum number of raindrops. The droplet growth due to coagulation is now efficient and raindrops start to fall out of the cloud. Nevertheless due to their relatively small size ($r_{max} < 170\,\mu m$) nearly all of them evaporate before reaching the ground. The cloud finally dissolves due to the fallout of the raindrops and intensive evaporation at the cloud edges.

Differences generated by the two different coagulation kernels develop after approximately 1400 s when the coagulation process is working efficiently. The development of the cloud with and without the influence of turbulence on the cloud microphysics is shown examplarily for the time $t = 1600$ s in Fig. 9.

Due to the short life span and the small amount of rain water content in the cumulus cloud, most properties of the cloud are only slightly affected by turbulence effects. Fig. 9 shows that the largest differences are evident for the raindrop quantities $N_{rain}$ and $q_{l,rain}$. The profiles of $q_{l,tot,cl}$ (Fig. 9 (c)) and $q_{l,rain,cl}$ (Fig. 9 (l)) indicate, that the values for the simulation with the turbulent coagulation kernel are slightly higher. The cross sections show, that the differences appear mainly in the upper part of the cloud. The differences of the raindrop properties between the two simulations are more distinct when looking at time series of the mean rain water path RWP= $\int_{surface}^{top} \rho q_{l,rain} dz$, the mean raindrop number density $N_{rain}$and the mean and maximum raindrop radius $\overline{r}_{rain}$ and $r_{max}$, as shown in Fig. 10. RWP and $N_{rain}$ are averaged over the whole model domain, $\overline{r}_{rain}$ over all grid volumes that contain raindrops. The results confirm, that after about 1450 s the simulation with a turbulent coagulation kernel produces more raindrops which result in a higher mean RWP. The mean and maximum raindrop radii show almost no differences. Thus the use of the turbulent coagulation kernel results in an enhanced formation of raindrops, whereas the typical size of the raindrops seems not to be affected very much.

In general, the effects of turbulence on the droplet formation in the cloud simulations are weaker than in the idealized simulations presented in Section 3. One reason could be the difference in the dissipation rate $\epsilon$ which is much smaller in the 3-D cloud than prescribed in the idealized simulations in Section 3. Therefore a weak influence of turbulence should be expected for the 3-D cloud simulation. However, earlier simulations by Riechelmann et al. (2012) showed a somewhat stronger influence of turbulence on cloud droplet formation, but note that the collision kernel from Ayala et al. (2008b) and Wang and Grabowski (2009) was used in this study. Furthermore, some preliminary comparisons with similar setups for single cumulus clouds by Riechelmann (2014) indicated, that the Ayala-Wang-kernel had a stronger influence on the droplet growth and rain formation than the Siewert-kernel discussed here. The quantification of the effect of the different turbulent collision kernels on the drop growth has to be left for further studies.

## 5 Summary and conclusions

We have investigated the influence of turbulence on the collisional growth of droplets in warm clouds by means of two models of different complexity with respect to description of the microphysical processes as well as with regard to the model geometry: a classical spectral BIN model embedded in a 0-D as well as 1-D geometry (BIN module in the RAINSHAFT model, c.f. Seifert and Beheng, 2001) and a recently developed Lagrangian cloud model (LCM, Riechelmann et al., 2012), which is based on the method of so called superdroplets (Andrejczuk et al., 2010; Shima et al., 2009). It should be noticed that turbulence was considered in terms of a recently derived parameterization of the collision kernel that has been obtained by a DNS model and extrapolated to conditions met in a wind tunnel experiment (see Siewert et al., 2014, referred to as Part I here). After presenting the basic description of the two microphysical modules BIN and LCM numerical results of different configurations are discussed: in the 0-D case the results obtained by considering pure coagulation only are analyzed whereas in the 1-D case coagulation is complemented by sedimentation mimicking a rain event. Finally results from an evolving cumuliform cloud in 3-D are shown.

Despite emphasis is placed on the turbulence impact, we first address differences appearing by the usage of the two different drop growth models: the quasi-stochastic growth model used in BIN and the continuous growth description in LCM (see discussion in Section 2.4). In the BIN calculations large drops are formed more rapidly than in the LCM modeling. This general result is found in the 0-D- and 1-D-simulations, and it occurs for all assumed turbulence intensities.

The evolutions of the drop ensembles following from the BIN and the LCM models and from the 0-D- and 1-D-simulations have in common that turbulence enhances the formation of larger drops with the turbulence dissipation rate $\epsilon$ as (a weak) controlling parameter: Whereas a moderate dissipation rate typical for atmospheric conditions leads only to a small acceleration of large drop formation, the more remarkable effect stems from application of a very large dissipation rate observed in the wind tunnel experiments described in Part I (here, the collision kernel is an extreme extrapolation).

An expensive 3D LCM simulation showed that turbulent enhancement is mostly negligible during the start

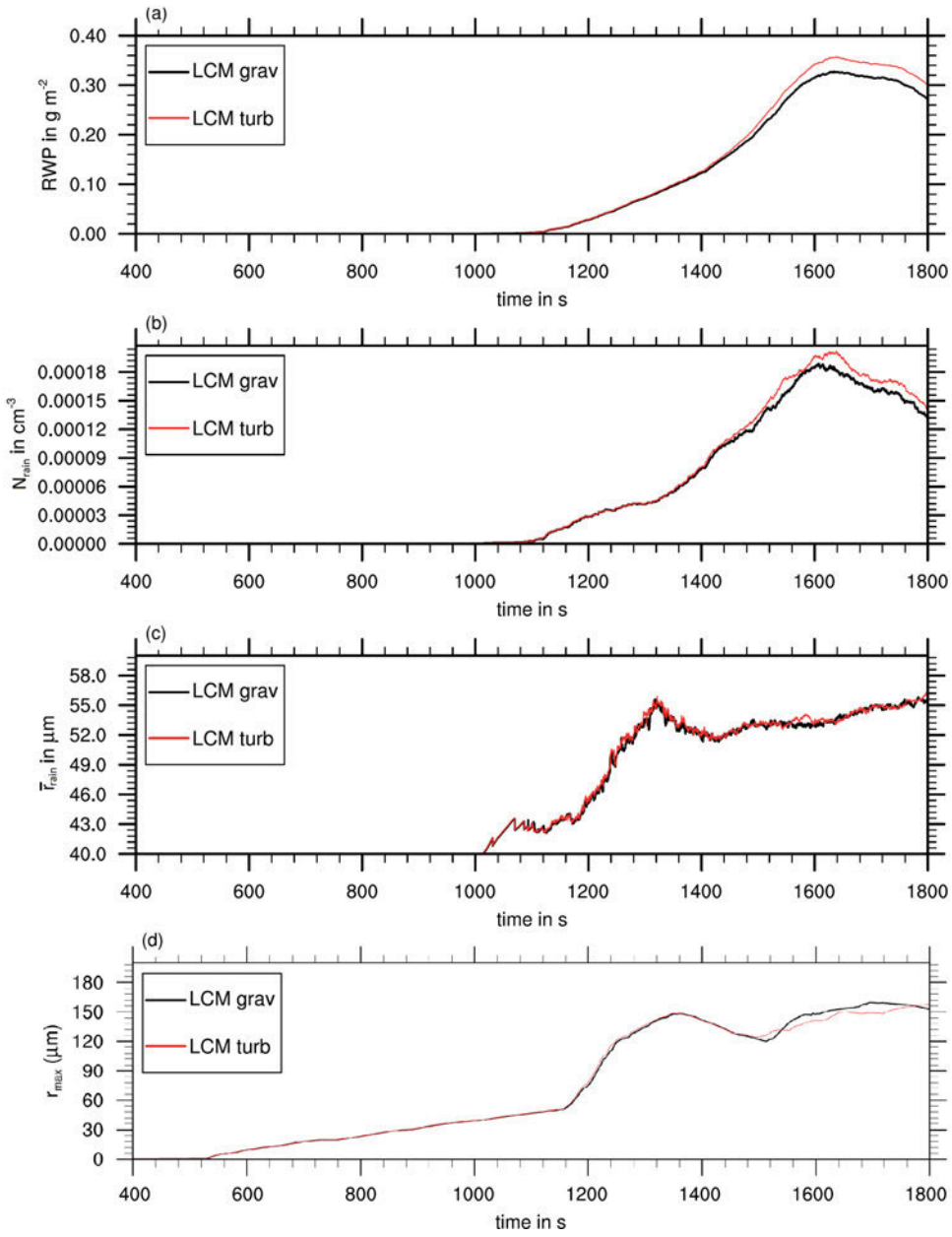


**Figure 10:** Time series of the mean rain water path RWP (a), the mean raindrop number density $N_{\text{rain}}$ (b), the mean raindrop radius $\overline{r}_{\text{rain}}$ (c) and the maximum raindrop radius $r_{\text{max}}$ (d). The values are averaged over the whole model domain, except for $\overline{r}_{\text{rain}}$, which is averaged over all grid volumes containing raindrops.

phase and remains relatively small in the final cloud stage, although the calculated dissipation rates are in the range of values measured in small cumulus clouds. This fact does not exclude that in very vigorous convective clouds, where relatively high dissipation rates (presumably amounting to several hundreds cm$^2$s$^{-3}$) may occur, these effects might be much more pronounced. But this conjecture has to be confirmed by observations not available to date.

In conclusion it can be stated that turbulence leads to an acceleration of the formation of larger droplets. However, the effect is weak for moderate turbulence intensities but can be remarkable for strong turbulence. The discrepancy between the results obtained by applying the spectral kinetic equation for droplet growth in the BIN model and the continuous description for the growth of super-droplets in LCM is relatively strong, hence more efforts should be made to match the results of both procedures with the BIN model as a reference. As outlined in Section 2.4, possible solutions may be to modify the continuous description by adding a new super-droplet characteristic in the LCM which includes a variance information for the droplet size or to exchange the continuous description by enabling the generation of new super-droplets during the coagulation process, similar to the method used by Andrejczuk et al. (2010). Furthermore, it seems necessary to increase the number of super-droplets in the large radius range to

overcome deficiencies in the population of large raindrops, e.g. by splitting those super-droplets into several ones with respectively smaller weighting factors. But as the computational resources increase with increasing super-droplet numbers, new methods for improving the speed up of LCMs, as proposed e.g. by Unterstrasser and Sölch (2013), have to be implemented. This task is now undertaken in a current project within the LES/LCM group of the co-author S. Raasch.

## Acknowledgments

We want to thank Yign Noh and Lian-Ping Wang for their helpful contributions to the improvement of the LCM. We also like to thank two anonymous reviewers for their very detailed comments which helped very much to improve the paper. This work was funded by the priority program SPP 1276 MetStröm by the Deutsche Forschungsgemeinschaft under grant ET 8/14, WA 1334/8, and BE 2081/10. The LCM simulations have been carried out on the Cray XC30 systems of the North-German Supercomputing Alliance (HLRN).

## Appendix A

The temporal change of the mass $M_n$ of all drops represented by the $n$-th super-droplet and of the weighting factor $A_n$ due to coagulation is calculated using a continuous growth model. A drop of radius $r_n$ and mass $x_n$ collides with smaller drops of radius $r_m$ and mass $x_m$, and swallows them. The mass growth rate is given in terms of the super-droplet model as:

$$\frac{dx_n}{dt} = \sum_{m=1}^{n-1} K(r_n, r_m) x_m \frac{A_m}{\Delta V} \tag{5.1}$$

The total mass $M_n$ increases by the collection of smaller drops. During one time step $\Delta t$, it is increased by:

$$(\Delta M_n)_{\mathrm{sd}} = \sum_{m=1}^{n-1} K(r_m, r_n)\, x_m \left[\frac{A_m}{\Delta V}\frac{A_n}{\Delta V}\right] \Delta V \Delta t\,, \tag{5.2}$$

The index *sd* stands for 'smaller drops'.

Mass $M_n$ is (partially) depleted by collection of the $n$-drops by larger ones:

$$(\Delta M_n)_{\mathrm{ld}} = \sum_{m=n+1}^{N_\mathrm{p}} K(r_m, r_n)\, x_n \left[\frac{A_m}{\Delta V}\frac{A_n}{\Delta V}\right] \Delta V \Delta t\,. \tag{5.3}$$

The index *ld* stands for 'larger drops'.

The new mass $M_n^*$ of all drops represented by the $n$-th super-droplet after one time step reads:

$$\begin{aligned} M_n^* &= M_n + (\Delta M_n)_{\mathrm{sd}} - (\Delta M_n)_{\mathrm{ld}} \\ &= A_n\, x_n + \sum_{m=1}^{n-1} K(r_m, r_n)\, x_m \left[\frac{A_m A_n}{\Delta V}\right] \Delta t \\ &\quad - \sum_{m=n+1}^{N_\mathrm{p}} K(r_m, r_n)\, x_n \left[\frac{A_m A_n}{\Delta V}\right] \Delta t\,. \end{aligned} \tag{5.4}$$

Note, that internal-coagulation does not change $M_n$.

The weighting factor $A_n$ is reduced due to depletion of drops. The collection of the $n$-drops by larger ones changes $A_n$ by

$$(\Delta A_n)_{\mathrm{ld}} = \sum_{m=n+1}^{N_\mathrm{p}} K(r_m, r_n) \left[\frac{A_m A_n}{\Delta V}\right] \Delta t\,. \tag{5.5}$$

Internal coagulation (index 'int') also reduces $A_n$:

$$(\Delta A_n)_{\mathrm{int}} = K(r_n, r_n) \frac{1}{2} \left[\frac{A_n (A_n - 1)}{\Delta V}\right] \Delta t \tag{5.6}$$

Accordingly, the weighting factor of the $n$-th super-droplet after one time step is:

$$\begin{aligned} A_n^* &= A_n - (\Delta A_n)_{\mathrm{int}} - (\Delta A_n)_{\mathrm{ld}} \\ &= A_n - K(r_n, r_n) \frac{1}{2} \left[\frac{A_n\,(A_n - 1)}{\Delta V}\right] \Delta t \\ &\quad - \sum_{m=n+1}^{N_\mathrm{p}} K(r_m, r_n) \left[\frac{A_m A_n}{\Delta V}\right] \Delta t\,. \end{aligned} \tag{5.7}$$

As the next step, we calculate the new drop mass $x_n^* = M_n^*/A_n^*$ from (5.7) and (5.4). For the spherically shaped drop the updated radius $r_n^*$ follows as

$$r_n^* = \left(\frac{3}{4\pi\rho_l} x_n^*\right)^{1/3}\,. \tag{5.8}$$

## Appendix B: Transformation of the drop size distribution function

Since mass $x$ and radius $r$ of spherically shaped drops are uniquely related, we can likewise give the drop size number distribution for mass intervals and for radius intervals, since the number of drops per volume with massed in the interval $dx$ around $x$ must be the same as that for drops with radii in the interval $dr$ around $r$ with $r = r(x)$, that is $f_\mathrm{r} dr = f_\mathrm{x} dx$. The index tells whether the size distribution is defined with respect to mass intervals or to radius intervals. The size distributions are simply related by

$$f_\mathrm{r} = f_\mathrm{x}\, 4\pi\rho_l r^2\,. \tag{5.9}$$

To illustrate the evolution of the drop ensemble, frequently a drop size mass distribution (also named mass density distribution) is introduced. Several possibilities are available for its definition. We select in this paper the following form. We transform $f_\mathrm{x}$ to the variable $\ln x$ as per $f_{\ln \mathrm{x}} d\ln x = f_\mathrm{x} dx$. Using the above definitions, the mass distribution can also be expressed by

$$x f_{\ln \mathrm{x}} = x^2 f_\mathrm{x}\,, \tag{5.10}$$

provided we refer to the increment $d\ln x$.

This definition of the drop mass size distribution has the advantage that when plotting as a function of drop

mass or radius, the contributions of the large drops are much more pronounced than in a plot of the number size distribution $f_x$ or $f_r$.

## References


Andrejczuk, M., W.W. Grabowski, J. Reisner, A. Gadian, 2010: Cloud aerosol interactions for boundary layer stratocumulus in the Lagrangian cloud model. – J. Geophys. Res. **115**, D22214.

Ayala, O., B. Rosa, L.-P. Wang, W. Grabowski, 2008a: Effects of turbulence on the geometric collision rate of sedimenting droplets. Part 1. Results from direct numerical simulation. – New J. Phys. **10**, 075015.

Ayala, O., B. Rosa, L.-P. Wang, 2008b: Effects of turbulence on the geometric collision rate of sedimenting droplets. Part 2. Theory and parameterization. – New J. Phys. **10**, 075016.

Beard, K., 1976: Terminal velocity and shape of cloud and precipitation drops aloft. – J. Atmos. Sci. **33**, 851–864.

Bordás, R., T. Hagemeier, B. Wunderlich, D. Thévenin, 2011: Droplet collisions and interaction with the turbulent flow within a two-phase wind tunnel. – Phys. Fluids **23**, 085105.

Bordás, R., V. John, E. Schmeyer, D. Thévenin, 2012: Measurement and simulation of a droplet population in a turbulent flow field. – Comput. Fluids **66**, 52–62.

Clift, R., J.R. Grace, M.E. Weber, 1978: Bubbles, Drops and Particles. – Academic Press, New York.

Gillespie, D., 1975: Three models for the coalescence growth of cloud drops. – J. Atmos. Sci. **32**, 600–607.

Grabowski, W., L.-P. Wang, 2013: Growth of cloud droplets in a turbulent environment. – Ann. Rev. Fluid Mech. **45**, 293–324.

Hall, W.D., 1980: A detailed microphysical model within a two-dimensional dynamic framework: Model description and preliminary results. – J. Atmos. Sci. **37**, 2486–2507.

Holland, J., E. Rasmusson, 1973: Measurement of atmospheric mass, energy, and momentum budgets over a 500-kilometer square of tropical ocean. – Mon. Wea. Rev. **101**, 44–55.

Hu, H., R. Srivastava, 1995: Evolution of raindrop size distribution by coalescence, breakup, and evaporation: Theory and observations. – J. Atmos. Sci. **52**, 1761–1783.

Katzwinkel, J., H. Siebert, T. Heus, R.A. Shaw, accepted: Measurements of turbulent mixing and subsiding shells in trade wind cumuli. – J. Atmos. Sci.

Kunnen, R.P.J., C. Siewert, M. Meinke, W. Schröder, K. Beheng, 2013: Numerically determined geometric collision kernels in spatially evolving isotropic turbulence relevant for droplets in clouds. – Atmos. Res. **127**, 8–21.

Lee, J.H., Y. Noh, S. Raasch, T. Riechelmann, L.-P. Wang, 2014: Investigation of droplet dynamics in a convective cloud using a lagrangian cloud model. – Meteor. Atmos. Phys. **124**, 1–21.

Mason, B.J., 1971: The Physic of Clouds. – Clarendon Press, Oxford.

Matheou, G., D. Chung, L. Nuijens, B. Stevens, J. Teixeira, 2011: On the fidelity of large-eddy simulation of shallow precipitating. – Mon. Wea. Rev. **139**, 2918–2939.

Pinsky, M., A. Khain, M. Shapiro, 2001: Collision efficiency of drops in a wide range of reynolds numbers: Effects of pressure on spectrum evolution. – J. Atmos. Sci. **58**, 742–764.

Pruppacher, H., J. Klett, 1997: Microphysics of clouds and precipitation. – Kluwer Academic Publishers, Dordrecht.

Raasch, S., M. Schröter, 2001: PALM – a large-eddy simulation model performing on massively parallel computers. – Meteorol. Z. **10**, 363–372.

Riechelmann, T., 2014: Untersuchungen zum Einfluss turbulenter Kollisionskernel auf die Entwicklung von konvektiven Wolken mit einem neu entwickelten Lagrangeschen Wolkenmodell. – Ph.D. Thesis (in German), Faculty of Mathematics and Physics, Leibniz University Hannover.

Riechelmann, T., Y. Noh, S. Raasch, 2012: A new method for large-eddy simulations of clouds with lagrangian droplets including the effects of turbulent collision. – New J. Phys. **14**, 065008.

Rogers, R.R., M.K. Yau, 1989: A Short Course in Cloud Physics. – Pergamon Press, Oxford.

Seifert, A., 2008: On the parameterization of evaporation of raindrops as simulated by a one-dimensional rainshaft model. – J. Atmos. Sci. **65**, 3608–3619.

Seifert, A., K.D. Beheng, 2001: A double-moment parameterization for simulating autoconversion, accretion and selfcollection. – Atmos. Res. **59-60**, 265–281.

Shima, S., K. Kusano, A. Kawano, T. Sugiyamaa, S. Kawaharab, 2009: The super-droplet method for the numerical simulation of clouds and precipitation: A particle-based and probabilistic microphysics model coupled with a non-hydrostatic model. – Quart. J. Roy. Meteor. Soc. **135**, 1307–1320.

Siebert, H., K. Lehmann, M. Wendisch, H. Franke, R. Maser, D. Schell, E.W. Saw, R.A. Shaw, 2006: Probing finescale dynamics and microphysics of clouds with helicopter-borne measurements. – Bull. Amer. Meteor. Soc. **87**, 1727–1738.

Siebesma, A.P., C.S. Bretherton, A. Brown, A. Chlond, J. Cuxart, P.G. Duynakerke, H. Jiang, M. Khairoutdinov, D. Lewellen, C.-H. Moeng, E. Sanchez, B. Stevens, D. Stevens, 2003: A large eddy simulation intercomparison study of shallow cumulus convection. – J. Atmos. Sci. **60**, 1201–1219.

Siewert, C., R. Bórdas, U. Wacker, K.D. Beheng, R.P.J. Kunnen, M. Meinke, W. Schröder, D. Thévenin, 2014: Influence of turbulence on the drop growth in warm clouds, Part I: Comparison of numerically and experimentally determined collision kernels. – Meteorol. Z., **23**, 397–410, DOI:10.1127/0941-2948/2014/0566

Unterstrasser, S., I. Sölch, 2013: Speeding up a Lagrangian ice microphysics code. – Geosci. Model Dev. Discuss. **6**, 3787–3817.

Vaillancourt, P., M. Yau, 2000: Review of particle-turbulence interactions and consequences for cloud physics. – Bull. Amer. Meteor. Soc. **81**, 285–298.

Wang, L.-P., W. Grabowski, 2009: The role of air turbulence in warm rain initiation. – Atmos. Sci. Lett. **10**, 1–8.

Wang, L.-P., O. Ayala, B. Rosa, W. Grabowski, 2008: Turbulent collision efficiency of heavy particles relevant to cloud droplets. – New J. Phys. **10**, 075013.

Xue, Y., L.-P. Wang, W. Grabowski, 2008: Growth of cloud droplets by turbulent collision-coalescence. – J. Atmos. Sci. **65**, 331–356.